

Bound-free $1^3\Pi \rightarrow 1^3\Sigma^+$ emission from the NaK molecule: Determination of the $1^3\Sigma^+$ repulsive wall above the dissociation limit

Mark Masters, John Huennekens, and Wei-Tzou Luh^{a)}
 Lehigh University, Department of Physics, Bethlehem, Pennsylvania 18015

Li Li,^{b)} A. Marjatta Lyyra,^{c)} Ken Sando,^{d)} Vassilios Zafirooulos,^{e)}
 and William C. Stwalley^{c)}

Center for Laser Science and Engineering, University of Iowa, Iowa City, Iowa 52242

(Received 11 December 1989; accepted 7 February 1990)

We report the observation of bound-free emission on the $1^3\Pi \rightarrow 1^3\Sigma^+$ band of the NaK molecule. The spectra, which consist of oscillating continua in the near-infrared, have been analyzed to determine parameters describing the repulsive wall of the $1^3\Sigma^+$ state above the dissociation limit. Spectra calculated using a potential of the form $Ae^{-BR} + C$ for the $1^3\Sigma^+$ state were compared to experimental spectra to yield the following values: $A = 5.94 \times 10^5 \text{ cm}^{-1}$, $B = 1.605 \text{ \AA}^{-1}$, $C = -220.520 \text{ cm}^{-1}$. This potential, which is referenced to the bottom of the RKR $1^3\Sigma^+$ well ($D_e = 209.1 \text{ cm}^{-1}$), is valid over the range $R = 3.4\text{--}4.5 \text{ \AA}$ ($R = 6.4\text{--}8.5 \text{ a.u.}$). The relative transition dipole moment of the $1^3\Pi \rightarrow 1^3\Sigma^+$ band has also been determined over a limited range in R ($7.5 < R < 8.9 \text{ a.u.}$) through the study of relative intensities of various maxima within each oscillating spectrum. In the simulated spectra, the dipole moment was represented by a functional form $D(R) = m(R - R_0) + D_0$ where D_0 was used to normalize the results to a recent theoretical calculation ($D_0 = 1.07 \text{ a.u.}$, $R_0 = 8.034 \text{ a.u.}$). The best fit for the parameter m was determined to be 0.121 ± 0.029 in atomic units.

I. INTRODUCTION

The lowest triplet state, $1^3\Sigma^+$, of the sodium-potassium molecule is mostly repulsive, but with a shallow van der Waals minimum at large internuclear separation. Bound-free fluorescence terminating on this state has been observed since 1978,¹⁻⁶ and these spectra have been used in several attempts to determine parameters describing the $1^3\Sigma^+$ repulsive wall above the dissociation limit.^{1,3,4,7,8} Interest in the repulsive $1^3\Sigma^+$ state of the alkali diatomics was piqued in 1980 by Konowalow and Julienne,⁹ who suggested that continuum fluorescence on the $1^3\Sigma_g^+ \rightarrow 1^3\Sigma_u^+$ bands of Li_2 and Na_2 might form the basis for continuously tunable near-infrared lasers.

Experimental observation of alkali triplet bands has been hindered by the dipole selection rule $\Delta S = 0$, and the fact that the ground state of all alkali diatomics is a singlet. This has made it difficult to selectively excite to a specific level of an upper triplet state. It is possible to populate these triplet states by means of collisions.⁵ However, this results in a great number of triplet levels being populated simultaneously and many interesting spectroscopic details are washed out in the complex fluorescence spectra. In particular, the first observation of the NaK $1^3\Pi \rightarrow 1^3\Sigma^+$ band was made in 1985.⁵ However, in this case, collisional population

of the $1^3\Pi$ state produced a fluorescence spectrum consisting of a broad featureless continuum, decreasing in intensity with increasing wavelength.

A more selective method used to populate the triplet states of the alkali diatomics has been to rely upon spin-orbit perturbations between nearby singlet and triplet levels of the same J .^{1-4,6,10-15} In NaK, for example, the $1^3\Pi$ and $2^1\Sigma^+$ states both dissociate to the sodium $3s$ plus potassium $4p$ atomic state limit. Because these two potentials overlap significantly (see Fig. 1), there are many possibilities for the occurrence of spin-orbit perturbations which can be used to

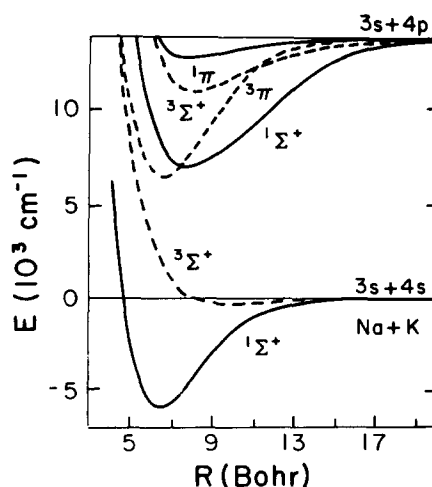


FIG. 1. Lowest six NaK molecular potential curves (from Ref. 28). Note that throughout the text the notation $2^1\Sigma^+$ refers to the second lowest $1^1\Sigma^+$ state, etc.

^{a)} Present address: Institute of Atomic and Molecular Science, Academia Sinica, P.O. Box 23-166, Taipei, Taiwan, 10764, Republic of China.

^{b)} Permanent address: Dalian Institute of Chemical Physics, Chinese Academy of Sciences, Dalian, People's Republic of China.

^{c)} Also Department of Chemistry and Department of Physics and Astronomy.

^{d)} Also Department of Chemistry.

^{e)} Permanent address: Foundation for Research and Technology, Hellas, P.O. Box 1527, Heraklion 71110, Crete, Greece.

populate the triplet. This is the approach used to gain access to the triplet manifold of states in the present work. Accurate spectroscopic constants for the NaK states $1^3\Pi_1$ and the bound portions of the $1^3\Sigma^+$, have previously been attained by way of similar $2^3\Pi-2^1\Pi$ state perturbations using the technique of perturbation-facilitated Fourier-transform spectroscopy.^{15,16} These experimental $1^3\Pi_1$ and $1^3\Sigma^+$ potentials, as well as those of the $1^1\Sigma^+$ and $2^1\Sigma^+$ states (which have also been mapped out using Fourier-transform spectroscopy in Refs. 16 and 17, respectively), play a significant role in the present analysis.

In a previous work, we reported observation of bound-free emission on the NaK $1^3\Pi \rightarrow 1^3\Sigma^+$ band where the $1^3\Pi$ state was populated via $2^1\Sigma^+ - 1^3\Pi$ spin-orbit perturbations following excitation by a multimode cw dye laser.⁶ Because of the large bandwidth (~ 30 GHz) of the multimode laser, it was impossible to avoid the simultaneous population of several v, J levels in the upper triplet state. This, and the complexity of the excitation spectra, rendered it impossible to make accurate assignments of the upper $1^3\Pi$ state levels responsible for the bound-free fluorescence. In addition, since several upper state levels were generally populated, some washing out of the spectra also occurred. Although bound-free oscillations were still visible, our inability to accurately label upper state levels made it impossible to use the spectra to determine specific information concerning the $1^3\Sigma^+$ potential.

In the present work, we report the observation of near-infrared bound-free emission from the $1^3\Pi_\Omega$ states ($\Omega = 0, 1, 2$) to the $1^3\Sigma^+$ state of the sodium-potassium molecule following single-mode ring dye-laser excitation to specific $1^3\Pi_\Omega(v, J)$ levels. Details of the experiment are presented in Sec. III. These observations of the bound-free $1^3\Pi \rightarrow 1^3\Sigma^+$ emission, and the previously determined potentials for the $1^1\Sigma^+$, $2^1\Sigma^+$, $1^3\Pi_1$, states, and the bound portion of the $1^3\Sigma^+$ state, have enabled us to map the repulsive wall of the $1^3\Sigma^+$ state above its dissociation limit, as a function of internuclear separation R (see Sec. IV C). From the fluorescence intensity versus wavelength, we have also been able to determine the relative transition dipole moment of the $1^3\Pi \rightarrow 1^3\Sigma^+$ band as a function of internuclear separation (Sec. IV D).

II. THEORY

NaK $1^3\Pi \rightarrow 1^3\Sigma^+$ bound-free emission from one upper v, J level forms a broad oscillatory continuum. Contained within each such fluorescence spectrum is much information about the lower state potential and the transition dipole moment $D(R)$. If the spectra can be successfully inverted, we can obtain accurate experimental constants for the $1^3\Sigma^+$ state repulsive wall and the function $D(R)$. Note that the accuracy with which bound state potentials can be mapped is a result of the hundreds or thousands of discrete lines in bound-bound spectra which can be used to fit the potentials. Repulsive states, on the other hand, are much more difficult to map because they generally result in diffuse continua. However, using a tunable laser to generate oscillating bound-free continua from many upper v, J levels, we can observe hundreds of maxima and minima which can be used

in a fitting procedure. Thus such spectra should be capable of producing experimental constants for repulsive state potentials with an accuracy approaching those obtainable for bound states.

In general, the intensity of bound-free emission within a range $d\lambda$ about λ is given by the following equation^{18,19}:

$$\frac{dI(\lambda)}{d\lambda} d\lambda = \frac{64}{3} \pi^4 c^2 N_u \lambda^{-6} T(\lambda) d\lambda, \quad (1)$$

where N_u is the number of atoms in the upper state level and

$$T(\lambda) = h \sum_{J', J''} S_{J', J''} \left[\int_0^\infty \chi_{v', J'}^{v', J'}(R) D(R) \chi_{L, J''}^{E_{L, J''}}(R) dR \right]^2. \quad (2)$$

Here $\chi_{v', J'}^{v', J'}(R)$ is the vibrational wave function in the upper bound energy level $E_{v'}$, and $\chi_{L, J''}^{E_{L, J''}}(R)$ is the energy normalized lower free state wave function corresponding to E_L . The $S_{J', J''}$ are Hönl-London factors, and $E_{v'} - E_L = hc/\lambda$. Information about either the upper or lower state potential is buried within the wave functions inside the integral. Note that in many cases (including the present one), $D(R)$ is a slowly varying function, so that it may be brought outside the integral in Eq. (2). Thus the important quantity in Eq. (2) is the square of the wave function overlap integral, $[\int_0^\infty \chi_{v'}^*(R) \chi_L(R) dR]^2$. Before going on to discuss the quantum mechanical calculations of these fluorescence spectra, it is useful to discuss two approximations to Eq. (2) which have been used to analyze bound-free spectra in the past.

In the classical Franck-Condon approximation (CFCA),²⁰ it is assumed that electronic transitions take place so rapidly that the nuclei do not change their relative position or velocity. This means that to each R value there is a corresponding wavelength which is given by the difference in the potentials at that R ; i.e., $\lambda(R) = hc [V_{v'}(R) - V_L(R)]^{-1}$. Thus, for a given wavelength, the integral in Eq. (2) collapses to a delta function in R (since $E_{v'}$ is fixed). Under the CFCA, bound-free emission is particularly simple when the difference potential is monotonic, since in that case there are no interference effects.²¹ This is the case for the NaK $1^3\Pi \rightarrow 1^3\Sigma^+$ band. The emission intensity at each wavelength is proportional to the probability that the atomic pair is separated by the appropriate R [given by $\chi_{v'}^*(R) \times \chi_{v'}(R)$ where $\chi_{v'}(R)$ is the upper state vibrational wave function]. Thus the CFCA spectra directly represent a reflection of the square of the upper state wave function onto the Mulliken difference potential,²¹ which is defined as the sum of the lower state potential and the upper state kinetic energy [see Fig. 2(a)]. By simply using the reflection principle of the CFCA in comparison with the experimental spectra, one could determine the NaK $1^3\Sigma^+$ state repulsive wall above the dissociation limit from the positions of the maxima and minima of the reflection structure. One could also determine the relative transition dipole moment from the relative intensities of the maxima.

A second approximation to Eq. (2) [which we will refer to as the delta function approximation—see Fig. 2(b)] can be obtained by replacing $\chi_L(R)$ by a delta function at the classical turning point⁷: $\chi_L(R) \sim \delta[E_L - V_L(R)]$. Since

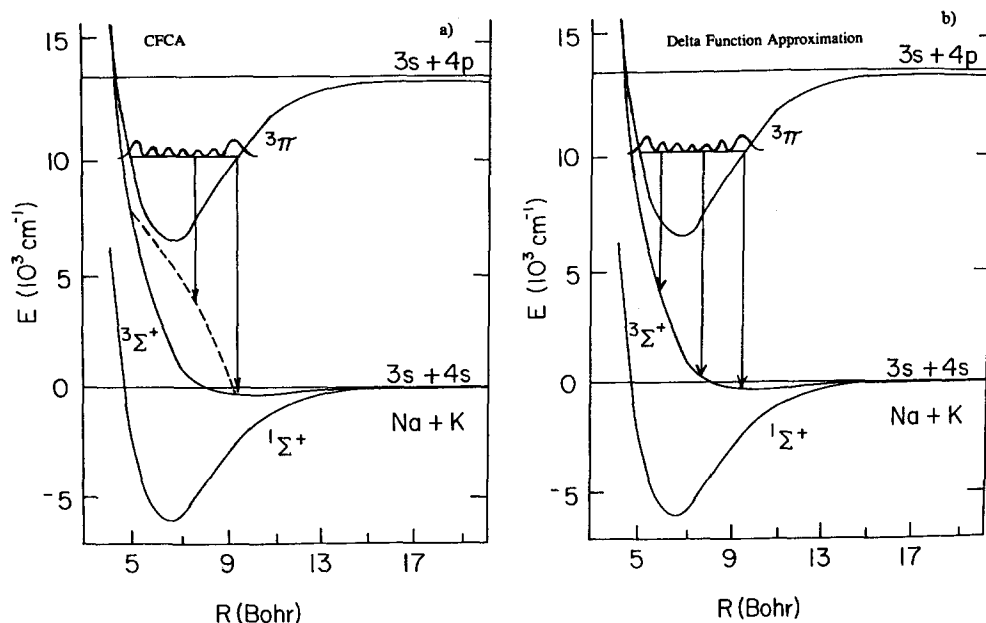


FIG. 2. (a) Origin of bound-free oscillatory spectra according to the CFCA, in which both position and kinetic energy are conserved. For each internuclear separation R there is a corresponding unique wavelength, and the intensity at that wavelength is proportional to the probability distribution in the bound upper state (sketched qualitatively in the figure). The dashed curve represents the lower state potential plus the upper state kinetic energy (Mulliken difference potential). Transitions at two R values are represented by arrows. (b) Oscillatory spectra according to the delta function approximation. Again the oscillations reflect the probability distribution of the upper state, but here the kinetic energy is not conserved. Instead the lower state wave function is represented by a delta function at the classical turning point.

the actual lower state wave function oscillates more rapidly with increasing kinetic energy, the overlap with the upper state wave function will tend to cancel for R values except near the repulsive wall. This delta function approximation exclusively weights the large maximum in the lower state wave function which occurs at the turning point. The delta function approximation, like the CFCA, is most accurate when the repulsive potential is steep and the bound state vibrational quantum number is low. Clearly, however, the delta function approximation is quite different from the CFCA, since the former does not conserve kinetic energy and therefore velocity during the transition.

Both the CFCA and the delta function approximation were tested for use in the inversion of the NaK $1^3\Pi \rightarrow 1^3\Sigma^+$ data by comparison of their results with fully quantum mechanical calculations of the spectra. (The quantum mechanical calculations were carried out using the program BOUND-FREE.¹⁸ These calculations are described more completely in Ref. 6.) Figure 3 shows such a comparison. Although both approximations reproduce the oscillatory structure, including the correct number of maxima, neither is sufficiently accurate in determining the positions of the maxima and minima for use in obtaining an improved $1^3\Sigma^+$ state experimental potential.

The difficulties encountered by the two approximation techniques described above can be traced to the fact that the overlap of the upper and lower state wave functions does not collapse to a delta function in R . In Fig. 4, following Tellinghuisen,²² we show the accumulated overlap integral as a function of R . From calculations of this type we found that the integrand of the overlap integral can be represented by a "square window." Rather than only a single R value contributing to the overlap integral as in the CFCA and the delta function approximation, the overlap builds up over some finite range of R which is a significant fraction of the width of the upper state well (typically on the order of 20%). Thus, with the fully quantum mechanical calculations, the transi-

tion dipole moment is much more difficult to determine because one cannot directly relate a specific R to each wavelength as in the CFCA or delta function approximation. The transition dipole moment at any R will affect the intensity over a fairly broad range of wavelengths, which can include several maxima of each oscillatory spectrum. In effect, one must deal with a moving average which is difficult to deconvolve. It is thus impossible to determine fine details within the transition dipole moment using these techniques. However, the finite width of this window does not cause any serious problems in the determination of the $1^3\Sigma^+$ repulsive wall above the dissociation energy because one does not need to directly relate wavelength to R in the fitting procedure. Problems of this nature and our results are discussed further in Secs. IV B through IV D.

III. EXPERIMENT

The experimental set-up is shown in Fig. 5. The sodium-potassium mixture was contained in a stainless-steel, five arm, crossed heat-pipe oven.²³ The oven was operated at about 360 °C with approximately 2 Torr of argon as a buffer gas. The oven temperature was such that it was near to, but short of, the conditions necessary for true heat-pipe operation.

A single-mode ring dye-laser with built in wavemeter (Coherent Autoscan CR-699-29), was used for the excitation of NaK. The ring laser, using LD700 dye, was pumped by ~ 7 W from a Kr^+ laser operating at 647.1 and 676.4 nm. This gave the dye laser a tuning range of approximately 700 to 780 nm with between 200 and 300 mW power. The laser wavelength was initially calibrated with the optogalvanic effect using a Ba hollow-cathode lamp.

Fluorescence was viewed at right angles to the laser excitation axis. Two monochromators were used to disperse the triplet ($1^3\Pi \rightarrow 1^3\Sigma^+$) and singlet ($2^1\Sigma^+ \rightarrow 1^1\Sigma^+$) fluorescence. The triplet fluorescence was resolved using a

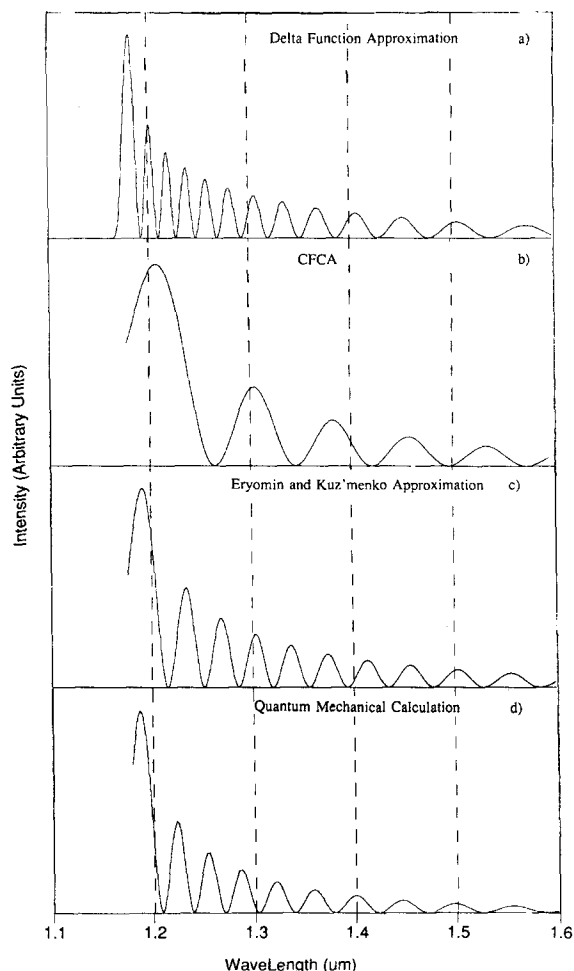


FIG. 3. Comparison of theoretical NaK $1^3\Pi_1(v' = 18, J' = 37) \rightarrow 1^3\Sigma^+$ emission calculated using four different methods: (a) delta function approximation, (b) CFCA, (c) Eryomin and Kuz'menko approximation, and (d) fully quantum-mechanical calculation. For all the calculations the experimental $1^3\Pi_1$, and bound portions of the $1^3\Sigma^+$ potential energy curves from Refs. 15 and 16 were used, in conjunction with the $1^3\Sigma^+$ repulsive wall determined in the present work. All four calculations predict the correct total number of oscillations which extend to very long wavelengths ($\sim 4.3 \mu\text{m}$). Here, the calculations were cut off at $1.6 \mu\text{m}$ corresponding to the cutoff of the detector sensitivity in the experiment.

0.22 m monochromator with 1 mm slits (giving a resolution of 7.2 nm), and was detected using a liquid-nitrogen cooled intrinsic germanium detector. The wavelength dependent relative triplet detection system efficiency was calibrated with a quartz-iodine lamp.²⁴ The correction of the triplet fluorescence spectra for the detection efficiency is important in the determination of $D(R)$ since that determination depends entirely upon relative intensities. A long-pass filter was used in front of each monochromator to block second and higher order diffractions from the gratings. Singlet band fluorescence was resolved using a 0.5 m monochromator with 150 μm slits (giving a resolution of 0.25 nm), and was detected with a photomultiplier of S-1 response. Both monochromators were calibrated with lines from the Ba hollow-cathode lamp.

We were able to take both excitation and fluorescence spectra by the use of two translating mirrors. The mirrors could be positioned to intercept the fluorescence and redi-

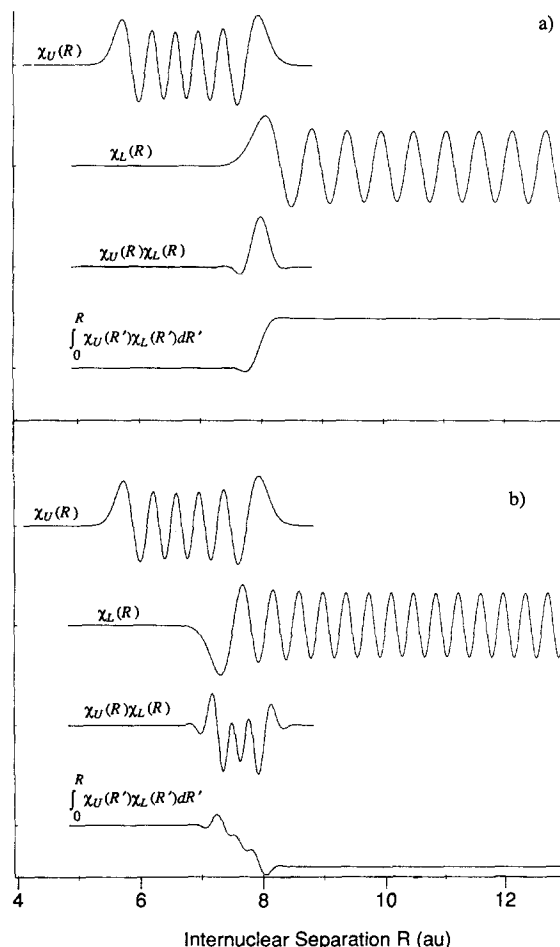


FIG. 4. Wave functions, integrand, and accumulated overlap integral for (a) the first and (b) the third maximum (from the left) of the spectrum shown in Fig. 12(d). The upper state level is $1^3\Pi_0(v' = 10, J' = 38)$. Note that the width of the region where the integral accumulates increases as it moves to smaller R values.

rect it to two free standing detectors. These were a Ge detector and a photomultiplier. The monochromators in this case were replaced by interference filters. The filter placed before the free-standing photomultiplier passed light from 0.65 to 1.0 μm . As a result, this detector acted as a monitor of the total singlet emission. The filter before the free-standing Ge detector passed light from 1.0 to 1.6 μm and therefore monitored the total triplet fluorescence. A beam splitter placed before the heat pipe sent a fraction of the laser beam to an iodine cell so we could continuously verify the accuracy of the wavemeter on extended laser scans. The laser was chopped at 200 to 300 Hz and the fluorescence signals were recorded using two lock-in amplifiers.

While using the free-standing detectors, we would scan the laser and observe the total triplet and total singlet fluorescence. The Autoscan laser data acquisition system is limited to three input data channels. One channel was used to acquire the vernier etalon scan, which was used to insure that no mode-hops occurred. The other two were used to acquire the three sets of data we were interested in observing: the total triplet fluorescence, total singlet fluorescence, and fluorescence from the I_2 cell. Thus we carried out two excita-

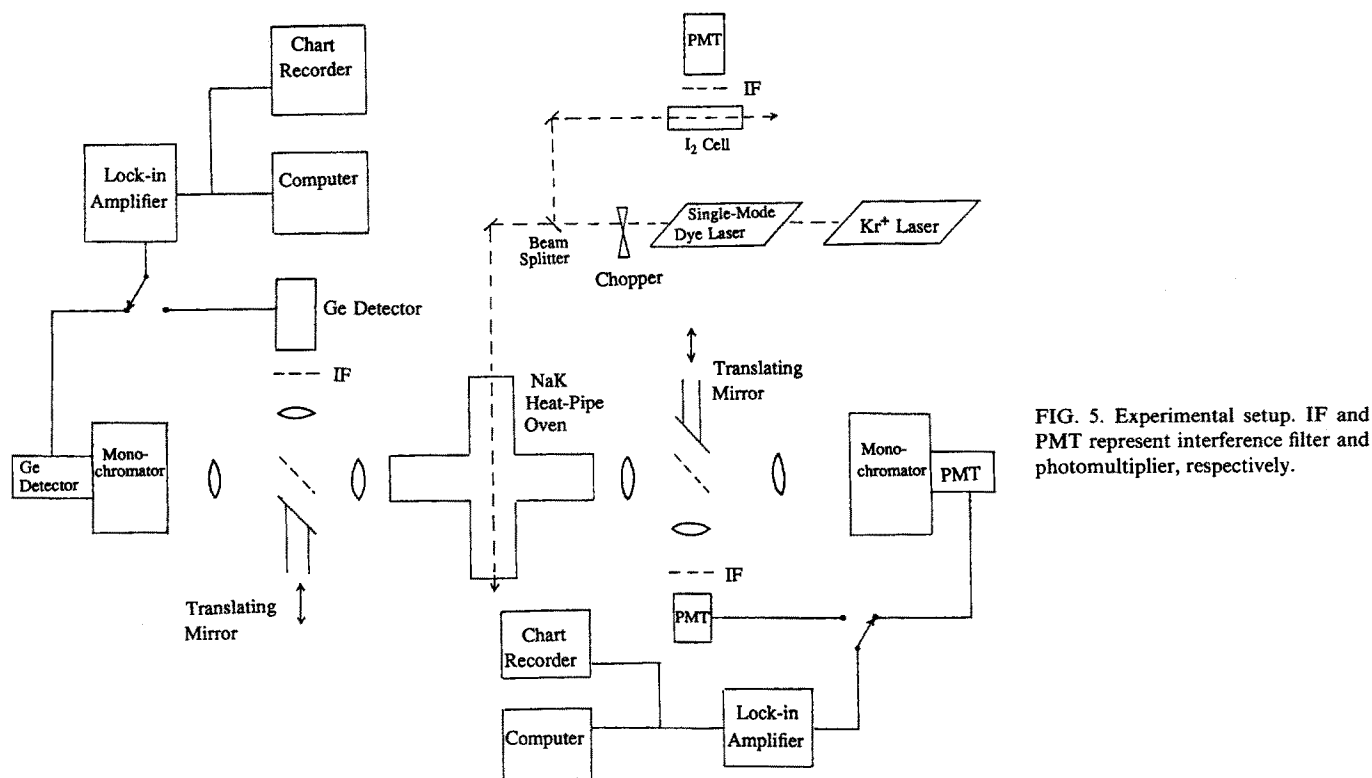


FIG. 5. Experimental setup. IF and PMT represent interference filter and photomultiplier, respectively.

tion scans in each region of interest. First, we would record an excitation scan of the singlet fluorescence with the I_2 signal. Then we would repeat the scan, recording the total triplet spectrum with the singlet spectrum. Following this, we would fix the laser wavelength to a position where the relative triplet to singlet intensity was high. Under these conditions, the laser was presumably tuned to a level with mostly triplet character. We would then translate the movable mirrors out of the way and record spectrally resolved fluorescence. Again two lock-ins were used. The excitation scans were directly recorded by the laser's computer, while the fluorescence spectra were recorded both on chart recorder and on computer.

IV. RESULTS

A. Spectra

Figure 6 shows an example of a composite excitation spectrum. Each spectrum contains an etalon scan, a total triplet fluorescence scan, a total singlet fluorescence scan, and an I_2 scan, each as a function of laser frequency. The total triplet fluorescence trace follows the total singlet, nearly peak for peak. This is due to collisional transfer from the pumped singlet level to nearby levels of the $1^3\Pi$ state. Occasionally a large triplet peak, corresponding to a level with a large triplet amplitude, was observed. Such peaks were used for fluorescence scans. Under these conditions, for fixed laser wavelengths, the resolved singlet spectra consists of series of P - R doublets extending from near the laser frequency to about $1.0\ \mu\text{m}$ (part of which is shown for one case in Fig. 7). The corresponding triplet spectra (see Fig. 8) consist of

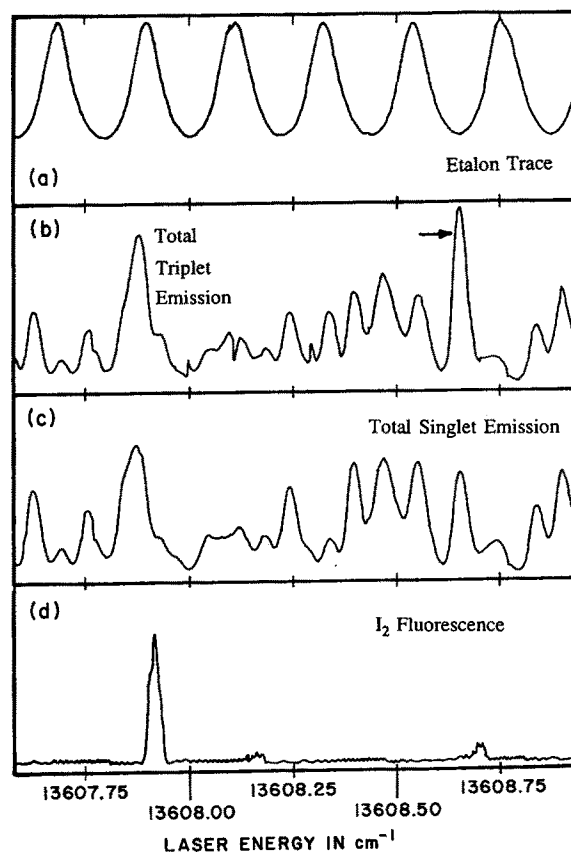


FIG. 6. Excitation spectra. (a) laser etalon signal indicating the continuity of the scan. (b) total triplet band emission. (c) total singlet emission. (d) I_2 fluorescence. The arrow in (b) indicates a position of enhanced triplet emission and therefore a perturbed energy level.

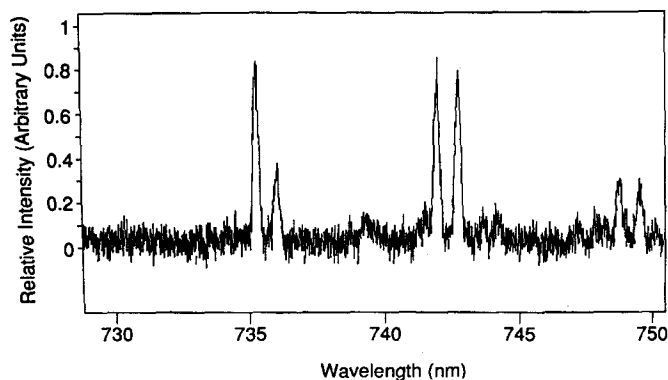


FIG. 7. P - R doublets of the downward $2^1\Sigma^+ (v' = 20, J' = 37) \rightarrow 1^1\Sigma^+ (v'', J'' = 36, 38)$ transitions. The upper state was pumped from the $v'' = 0, J'' = 36$ level of the $1^1\Sigma^+$ state. Typically these P - R doublets extend to approximately $1.0 \mu\text{m}$.

oscillatory continua, which are characteristic of bound-free reflection structure.

The singlet spectra can be assigned to the NaK molecule after measuring the energy separations between adjacent P - R doublets. The energy separation between the lines depends entirely upon the energy levels of the NaK ground state. The ground states of NaK, K_2 and Na_2 (which are all present in the vapor) are sufficiently different to allow distinction. (In fact, almost all observed fluorescence signals could be assigned to NaK. This is because potassium tends to be pushed out of the central region of the oven where the fluorescence is produced, so that the K_2 concentration is low in that region. In addition, Na_2 does not absorb strongly at these excitation wavelengths.) The triplet bound-free emission can be unambiguously assigned to NaK since the analogous $1^3\Pi \rightarrow 1^3\Sigma^+$ transitions in Na_2 and K_2 are forbidden by symmetry considerations. (The analogous states in the homonuclear molecules are designated as $1^3\Pi_u$ and $1^3\Sigma_u^+$, and $u \rightarrow u$ transitions are strictly forbidden.) Since all signals are linear in laser power, the upper state must lie in the first excited manifold of states.

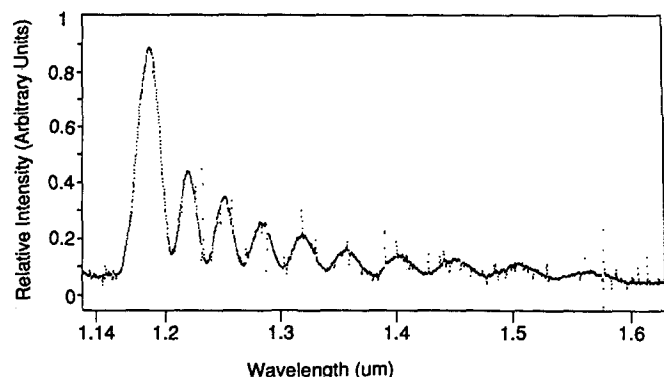


FIG. 8. Bound-free emission from the $1^3\Pi_1 (v' = 18, J' = 37)$ level. This spectrum was obtained with the same pump wavelength used to produce Fig. 7.

B. Analysis of spectra

The excitation spectra are very complex since there are so many thermally populated levels of the ground state. In general, these spectra were used simply to locate levels with a large triplet amplitude.

In order to assign v and J for the pumped $1^3\Pi$ level, which were needed to model the bound-free emission, we analyzed the associated singlet band emission. Since levels which produce enhanced triplet fluorescence are spin-orbit perturbed, these $1^3\Pi_\Omega$ levels have an admixture of $2^1\Sigma^+$ probability amplitude which allows population from the ground state. This $2^1\Sigma^+$ amplitude also results in downward transitions to the $1^1\Sigma^+$ state [$2^1\Sigma^+ (v'', J'') \rightarrow 1^1\Sigma^+ (v'', J' \pm 1)$] obeying the selection rule, $\Delta J = \pm 1$. The singlet spectra consist of a series of P - R doublets (see Fig. 7) which can be analyzed to yield the assignments of v'' and J' . In particular the P and R line splitting within a doublet roughly identifies J' , while the splitting between doublets yields the various values of v'' . In practice, both quantities depend upon both v'' and J' , so assignments were made by comparison of a list of $1^1\Sigma^+ (v'', J' - 1)$, $1^1\Sigma^+ (v'', J' + 1)$ energy differences with the observed P - R splittings, and by comparison of a list of $1^1\Sigma^+ (v'', J'')$, $1^1\Sigma^+ (v'' + 1, J'')$ energy differences with observed splittings between doublets. The energy differences were generated from the constants of Ref. 16.

Once the assignments of J' and the various v'' were made, it was easy to determine the level of the ground state which was pumped by the laser. A search program identified all possible levels of the $2^1\Sigma^+$ state which could be pumped from the initial $1^1\Sigma^+$ rovibrational level given the laser wavelength, the unperturbed $2^1\Sigma^+$ level energies (from Ref. 17), and an energy error or tolerance. The energy error, typically chosen to be 5 cm^{-1} , was needed to cover possible perturbation-induced deviations from the unperturbed energy positions.

Since the $2^1\Sigma^+ - 1^3\Pi$ perturbations only involve states of the same J , it is straightforward to assign the Ω , v , and J values to the mixed state's $1^3\Pi_\Omega$ probability amplitude. This was done using a second search program which found the closest unperturbed $1^3\Pi_\Omega$ level with the same J' value as the pumped $2^1\Sigma^+$ level. We identified triplet emission from all fine-structure levels of the $1^3\Pi$ state. However, most of the spectra analyzed involved $1^3\Pi_0 - 2^1\Sigma^+$ perturbations which give rise to the strongest triplet fluorescence. This is because the spin-orbit operator only couples the $2^1\Sigma^+$ levels to those of the $1^3\Pi_0$. The $2^1\Sigma^+$ levels are also coupled to $1^3\Pi_1$ and $1^3\Pi_2$ levels, but only through more complex secondary perturbations. Table I shows the v, J levels of the $1^1\Sigma^+$, $2^1\Sigma^+$, and $1^3\Pi_\Omega$ states which were coupled by the laser for specific pump wavelengths.

As an additional check, we verified that the observed shift of a mixed level from its unperturbed position was consistent with the assigned perturbation; i.e., that the higher of the two levels was shifted up in energy or the lower of the two levels shifted down. We found that most of the chosen pumped levels were perturbed triplets (triplet amplitude greater than singlet amplitude) since these levels generally give rise to the largest triplet fluorescence.

TABLE I. NaK levels coupled by the laser for specific pump frequencies which produced spectra analyzed in the present work. In each case, the initial state is $1^1\Sigma^+(v,J)$ with v and J given in the table. The final state is an admixture of $2^1\Sigma^+(v,J)$ and $1^3\Pi_\Omega(v,J)$ levels with Ω , v , and J given in the table for both components. ($\Omega = 0$ for the $2^1\Sigma^+$ state.)

| Laser energy (cm^{-1}) | $1^1\Sigma^+$ (v,J) | $2^1\Sigma^+$ (v,J) | $1^3\Pi$ (Ω,v,J) |
|--------------------------------------|----------------------------|----------------------------|------------------------------|
| 13 949.88 | 4,45 | 32,46 | 1,26,46 |
| 13 788.32 | 1,30 | 24,31 | 0,21,31 |
| 13 698.69 | 0,27 | 21,28 | 0,19,28 |
| 13 606.73 | 0,36 | 20,37 | 1,18,37 |
| 13 572.00 | 0,47 | 20,46 | 0,18,46 |
| 13 569.45 | 0,63 | 21,62 | 1,18,62 |
| 13 488.05 | 0,23 | 18,24 | 0,17,24 |
| 13 269.68 | 0,15 | 15,16 | 0,15,16 |
| 12 939.08 | 0,37 | 11,38 | 0,12,38 |
| 12 713.26 | 0,37 | 8,38 | 0,10,38 |

The largest error in the above procedure results from inaccuracy in the $1^3\Pi_0$ state constants which were used in predicting the unperturbed energies for that state. These constants were derived from the highly accurate $1^3\Pi_1$ state constants of Ref. 15, together with the measured fine-structure constant from the same reference:

$$\begin{aligned} & \{E[1^3\Pi_1(v,J)] - E[1^3\Pi_0(v,J)] \\ & = 15.557 \text{ cm}^{-1} - 0.0112(v + \frac{1}{2}) \text{ cm}^{-1}\}. \end{aligned}$$

This is not very satisfactory for our purposes, and we estimate that neglect of higher order terms leads to an error of as much as 1 cm^{-1} in the unperturbed $1^3\Pi_0$ energies. (This estimate was made by comparing calculated energies for the $1^3\Pi_2$ levels using the $1^3\Pi_1$ level energies and the fine-structure constant of Ref. 15, with more accurate values which include higher order terms.²⁵) This uncertainty has a negligible effect on our determination of the $1^3\Sigma^+$ repulsive wall (see next section), but makes it difficult to study the perturbations themselves.

In principle, it should be possible to determine the electronic contribution to the spin-orbit interaction matrix element ξ_{el} ¹⁴:

$$\langle \Psi_{1^3\Pi_0} | H_{SO} | \Psi_{2^1\Sigma^+} \rangle = \xi_{el} \langle \chi_{1^3\Pi_0} | \chi_{2^1\Sigma^+} \rangle, \quad (3)$$

where $\Psi_{1^3\Pi_0}$ and $\Psi_{2^1\Sigma^+}$ are the total molecular wave functions, and the χ 's are vibrational wave functions. By ignoring interactions between $1^3\Pi_{2,1}$ and $1^3\Pi_0$ levels, we can construct a simple interaction matrix involving only the $1^3\Pi_0$ and $2^1\Sigma^+$ states²⁶:

$$\begin{pmatrix} E_\Sigma & \xi_{el} \langle \chi_{1^3\Pi_0} | \chi_{2^1\Sigma^+} \rangle \\ \xi_{el} \langle \chi_{2^1\Sigma^+} | \chi_{1^3\Pi_0} \rangle & E_{II} \end{pmatrix}, \quad (4)$$

where E_Σ and E_{II} are the unperturbed energies. Diagonalizing the matrix gives an expression for the perturbed energies, E_+ and E_- ²⁶:

$$\begin{aligned} E_\pm & = \frac{E_{II} + E_\Sigma}{2} \pm \frac{1}{2} \left[(E_{II} - E_\Sigma)^2 \right. \\ & \left. + 4\xi_{el}^2 |\langle \chi_{1^3\Pi_0} | \chi_{2^1\Sigma^+} \rangle|^2 \right]^{1/2}. \end{aligned} \quad (5)$$

Determination of ξ_{el} therefore requires knowledge of three of the four quantities, E_Σ , E_{II} , E_+ , and E_- . In the present experiment, we accurately know one of the perturbed energies and E_Σ . Unfortunately, we were unable to locate the second perturbed level with the techniques employed. This, combined with the above mentioned uncertainties in E_{II} , made it possible to determine ξ_{el} accurately, since a perturbation typically results in a shift only of 0.5 cm^{-1} .¹⁴ Work to further investigate these perturbations is currently in progress.

C. Determination of the $1^3\Sigma^+$ potential above the dissociation energy

Having determined the particular rovibrational level of the $1^3\Pi_\Omega$ state which was populated at a specific laser wavelength through perturbations with the $2^1\Sigma^+$ state, we could proceed with the determination of the $1^3\Sigma^+$ repulsive wall above the dissociation limit. Our procedure was to assume a repulsive potential of a certain form with free parameters, quantum mechanically simulate the oscillatory spectra using this potential, and vary the parameters of the potential to obtain the best agreement between observed and calculated spectra (i.e., positions of the oscillatory maxima and minima). We chose to fit the repulsive wall by a function of the form $Ae^{-BR} + C$. This form for $V(R)$ was used previously by LeRoy *et al.*⁸ to describe this same $1^3\Sigma^+$ repulsive potential in a fit of bound-free fluorescence from a higher triplet state ($2^3\Pi$). In their work, the fitted potential was required to join smoothly with the experimentally determined bound portion of the $1^3\Sigma^+$ state¹⁶; i.e., both the function and its first derivative were made continuous at the junction. This effectively reduced the fit to one parameter, since the continuity of the potential, and the continuity of the derivative each eliminated one degree of freedom. The final free parameter was then obtained by requiring the best match to the spectra. We attempted to obtain "one-parameter" fits using the forms $Ae^{-BR} + C$ and $(A/R)e^{-BR} + C$. However, we were unable to obtain a good match (within experimental error) to observed spectra from both high and low v levels of the $1^3\Pi$ state using the same values for the parameters. In order to fit all of our data, we dropped the requirement of a continuous derivative of the repulsive wall potential with the known $1^3\Sigma^+$ bound well. This resulted in what is effectively a two-parameter fit. We believe this is acceptable since our data do not detail the region of the "wall" to well junction.

The simulations of the bound-free spectra were fully quantum mechanical and were carried out for the specific levels of the $1^3\Pi_\Omega$ state which were previously determined to be the levels pumped in the experiment. The calculations were carried out using the program BOUND-FREE.^{18,19} The program utilized the assumed form of the $1^3\Sigma^+$ repulsive wall in conjunction with the experimental $1^3\Pi_\Omega$, and bound portion of the $1^3\Sigma^+$ potential energy curves. These latter two were calculated using a spline fit to the RKR rotationless potentials obtained from the experimentally determined term values in Refs. 15 and 16. For the $1^3\Pi_\Omega$ states, we determined turning points for $v = -\frac{1}{2}$ to 50, yielding a range in R of 2.5145 to 5.7223 Å. For the $1^3\Sigma^+$, we deter-

mined turning points for $\nu = -\frac{1}{2}$ to $\nu = 11$, yielding a range in R of 4.6452 to 9.0780 Å. These RKR turning points are given in Table II. We limited the inner turning point of the $1^3\Sigma^+$ state to $R = 4.6452$ Å (corresponding to $\nu = 6$) because at R 's near the dissociation energy, the turning points become unreliable as generated by the RKR procedure.⁸ P , Q , and R transitions were all included in the simulations, which causes a slight broadening of the oscillatory maxima, but little change in intensity at the minima. However, the instrument function of the monochromator does significantly increase the intensity at the minima in the experimental spectra. In order to take this into account, we convoluted the simulated spectra with a triangular instrument function of 7.2 nm full width half-maximum, corresponding to the measured monochromator resolution. This procedure resulted in good agreement of the intensities at the minima. Each simulated spectrum involved calculation of the intensity at 200 wavelengths to cover the observed region. Because we were simulating spontaneous emission dispersed on a linear wavelength scale, a weighting factor of λ^{-6} was used [see Eq. (1)]. All calculations were made using a theoretical determination of the transition dipole moment, $D(R)$,²⁷ since the experimental transition dipole moment function was yet to be determined. The effect of using this theoretical $D(R)$ was later seen to shift the calculated peak positions by an amount which was less than our experimental error.

For each simulation, the parameters A and B were estimated, while C was determined by tying on to the $1^3\Sigma^+$ experimental potential at $R = 4.6452$ Å. A and B were then varied until the simulations were consistent with our data. This procedure converged fairly quickly since the effects of the $1^3\Sigma^+$ state repulsive wall parameters were very clear in

the calculations. If the oscillations in the calculated spectrum were too spread out at short wavelength, then the trial $1^3\Sigma^+$ state wall was not sufficiently steep. Conversely, if the oscillations in the calculated spectrum were too close at short wavelength, then the trial potential was too steep. Our reported best fit potential was, of course, required to simultaneously fit all analyzed experimental spectra within experimental error.

We found that in the present case, the emission from higher ν levels of the $1^3\Pi_0$ states was less sensitive to the shape of the $1^3\Sigma^+$ potential, over the range of R studied, than emission from lower ν levels. This is because all information about the shape of the $1^3\Sigma^+$ potential repulsive wall is contained within the lower ($1^3\Sigma^+$) state wave function $\chi_L(R)$, which is most sensitive to the shape of the potential for R values near the turning point. {The oscillation wavelength of $\chi_L(R)$ is determined by the kinetic energy $p^2/(2m)$ at R , and the de Broglie relation $\lambda = h/p$. Relative changes in λ due to changes in $V(R)$ [and therefore $p^2/(2m)$ at R] are greatest when kinetic energy is smallest; i.e., near the turning point. Alternatively, looking at it from a mathematical standpoint, the solution to the Schrödinger equation for the lower state wave function $\chi_L(R)$ is most sensitive to the boundary conditions for positions near the boundary.} In the present case, for higher ν' levels, the principal contribution to the intensity at λ comes from larger R values and thus from regions farther from the $1^3\Sigma^+$ repulsive wall. Therefore our derived potential is most sensitive to spectra obtained from the lower ν' levels. In the more general case, the repulsive potential at R is most accurately determined by emission from a bound vibrational state with either of its turning points (inner or outer) close to R .

TABLE II. RKR turning points for the $1^3\Sigma^+$, $1^3\Pi_1$, and $1^3\Pi_0$ states of NaK calculated from the constants of Refs. 16 and 15, respectively. The energy zeros of the $1^3\Sigma^+$ and $1^3\Pi_1$ are with respect to the bottom of each well. The bottom of the $1^3\Pi_0$ state is with respect to the $1^3\Pi_1$, zero. These RKR potentials were used in the quantum mechanical simulations of the $1^3\Pi_0 \rightarrow 1^3\Sigma^+$ bound-free emission.

| ν | $1^3\Sigma^+$ | | $D_e = 209.1 \text{ cm}^{-1}$ | | | $1^3\Pi_1$ | | $1^3\Pi_0$ | |
|-------|---------------|-----------------------------|-------------------------------|---------------|-----------------------------|---------------|-----------------------------|------------|--|
| | $R(\text{Å})$ | Energy (cm^{-1}) | ν | $R(\text{Å})$ | Energy (cm^{-1}) | $R(\text{Å})$ | Energy (cm^{-1}) | | |
| 6 | 4.6452 | 122.945 401 | 45 | 2.5339 | 4711.961 397 | 2.5339 | 4696.913 997 | | |
| 5 | 4.6886 | 107.526 156 | 40 | 2.5700 | 4280.095 498 | 2.5700 | 4264.992 098 | | |
| 4 | 4.7403 | 90.822 054 | 35 | 2.6113 | 3823.133 155 | 2.6113 | 3807.973 755 | | |
| 3 | 4.8027 | 72.842 288 | 30 | 2.6586 | 3343.438 421 | 2.6587 | 3328.223 021 | | |
| 2 | 4.8804 | 53.596 053 | 25 | 2.7134 | 2842.775 852 | 2.7134 | 2827.504 452 | | |
| 1 | 4.9848 | 33.092 543 | 20 | 2.7777 | 2322.453 075 | 2.7777 | 2307.125 675 | | |
| 0 | 5.1567 | 11.340 952 | 15 | 2.8550 | 1783.432 583 | 2.8550 | 1768.049 183 | | |
| -1/2 | 5.4834 | 0.000 000 | 10 | 2.9524 | 1226.412 730 | 2.9524 | 1210.973 330 | | |
| 0 | 5.8008 | 11.340 952 | 5 | 3.0877 | 651.877 947 | 3.0877 | 636.382 547 | | |
| 1 | 6.1271 | 33.092 543 | 0 | 3.3669 | 60.118 160 | 3.3669 | 44.566 760 | | |
| 2 | 6.3925 | 53.596 053 | -1/2 | 3.5045 | 0.000 000 | 3.5045 | -15.557 000 | | |
| 3 | 6.6400 | 72.842 288 | 0 | 3.6455 | 60.118 160 | 3.6455 | 44.566 760 | | |
| 4 | 6.8837 | 90.822 054 | 5 | 4.0229 | 651.877 947 | 4.0229 | 636.382 547 | | |
| 5 | 7.1316 | 107.526 156 | 10 | 4.2608 | 1226.412 730 | 4.2608 | 1210.973 330 | | |
| 6 | 7.3896 | 122.945 401 | 15 | 4.4655 | 1783.432 583 | 4.4655 | 1768.049 183 | | |
| 7 | 7.6638 | 137.070 593 | 20 | 4.6555 | 2322.453 075 | 4.6555 | 2307.125 675 | | |
| 8 | 7.9606 | 149.892 540 | 25 | 4.8388 | 2842.775 852 | 4.8387 | 2827.504 452 | | |
| 9 | 8.2878 | 161.402 046 | 30 | 5.0203 | 3343.438 421 | 5.0202 | 3328.223 021 | | |
| 10 | 8.6555 | 171.589 916 | 35 | 5.2040 | 3823.133 155 | 5.2039 | 3807.973 755 | | |
| 11 | 9.0780 | 180.446 958 | 40 | 5.3938 | 4280.095 498 | 5.3937 | 4264.992 098 | | |
| | | | 45 | 5.5945 | 4711.961 397 | 5.5943 | 4696.913 997 | | |

From detailed comparison of simulated and observed NaK $1^3\Pi \rightarrow 1^3\Sigma^+$ spectra, we report our best fit for the $1^3\Sigma^+$ repulsive wall potential of the form $V(R) = Ae^{-BR} + C$: $A = 5.94 \times 10^5 \text{ cm}^{-1}$, $B = 1.605 \text{ \AA}^{-1}$, $C = -220.520 \text{ cm}^{-1}$. This potential is referenced to the bottom of the RKR $1^3\Sigma^+$ well, given in Table II ($D_e = 209.1 \text{ cm}^{-1}$), and is valid for $3.4 < R < 4.5 \text{ \AA}$ ($6.4 < R < 8.5 \text{ a.u.}$). We note that because we are only able to observe the bound-free emission out to about $1.6 \mu\text{m}$ with the intrinsic germanium detector, we can only accurately map the $1^3\Sigma^+$ potential to a point $\sim 2000 \text{ cm}^{-1}$ above the dissociation energy. [This limit is obtained by subtracting the energy of a $1.6 \mu\text{m}$ photon from the energy of the highest $1^3\Pi_\Omega$ level producing observed and analyzed emission.]

In Fig. 9 we have compared our experimental $1^3\Sigma^+$ repulsive wall with those of LeRoy *et al.*⁸ and Kato and Noda⁴ and with the calculated potentials of Stevens *et al.*²⁸ and Jeung *et al.*²⁹ The filled area (i.e., heavy solid curve) in Fig. 9 shows the estimated uncertainty of our experimental potential. Parameters outside this range predict spectra which disagree with our observations by more than the experimental uncertainties.

It can be seen that the $1^3\Sigma^+$ potential determined in the present work is in reasonable agreement with that of Kato and Noda⁴ (obtained from their analysis of $2^3\Pi \rightarrow 1^3\Sigma^+$ band bound-free emission) but disagree significantly with that of LeRoy *et al.* who used the uniform harmonic approximation^{7,8} to analyze the $2^3\Pi \rightarrow 1^3\Sigma^+$ spectrum obtained by Breford and Engelke.¹ This latter discrepancy is significant given that the uniform harmonic approximation has been shown to yield accurate results when

used to invert synthetic spectra. However, we do not believe this discrepancy is an indication of any problem with this method. Rather, in the case of the NaK $2^3\Pi \rightarrow 1^3\Sigma^+$ band analyzed by LeRoy *et al.*⁸ neither the upper nor lower state potentials was assumed known in the inversion. Thus the analysis of the bound-free emission yielded an infinite family of pairs of possible upper and lower state potentials. Choice among these possible pairs of states was made by considering also the bound-bound emission into the $1^3\Sigma^+$ van der Waals well. In the analysis, the $1^3\Sigma^+$ potential was represented by $V(R) = Ae^{-BR} + C$ where B was a free parameter and A and C were fixed by requiring continuity of the potential and its derivative with the known bound portion of the $1^3\Sigma^+$ potential. LeRoy *et al.* found that bound state energies and bound-bound transitions were in best agreement with observation when B was chosen to be 1.68 or 1.80 \AA^{-1} . However, their analysis did not rule out the possibilities that $B = 1.52$ or 2.27 \AA^{-1} might be correct, since these values also gave local minima in bound state energy discrepancies.⁸ We have found that the potential obtained using $B = 2.27 \text{ \AA}^{-1}$ is actually in fairly good agreement with the potential determined in the present work. However, as stated earlier, we were unable to fit both our high and low ν data within uncertainties with a one-parameter potential such as that used by LeRoy.

The discrepancy between the present result and that of LeRoy *et al.* for the $1^3\Sigma^+$ potential is also consistent with a similar discrepancy between LeRoy's $2^3\Pi$ potential and that recently obtained experimentally by Kowalczyk.³⁰ Kowalczyk (whose $2^3\Pi$ potential is in good agreement with that of Kato and Noda⁴), found the inner turning point for

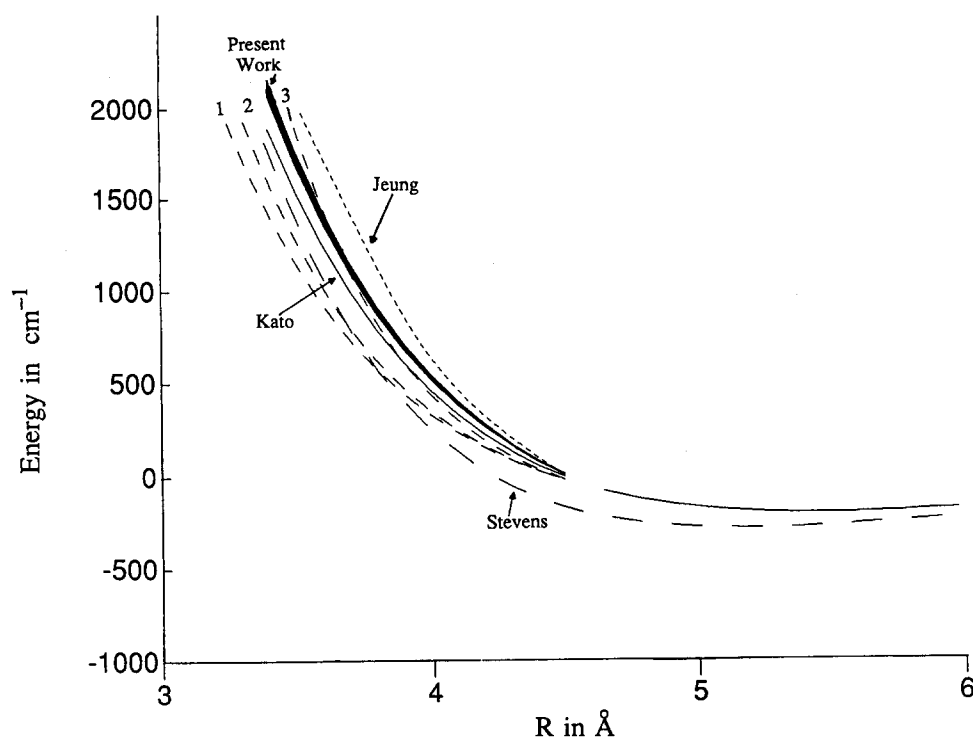


FIG. 9. A comparison of the $1^3\Sigma^+$ repulsive wall (including range of uncertainty) obtained in the present work (filled area or heavy solid line), with those determined by Kato and Noda (Ref. 4) (thin solid line), and by LeRoy *et al.*⁸ (The two medium dashed lines labeled 1 and 2, corresponding to LeRoy's β parameter equal to 1.68 and 1.80 \AA^{-1} , respectively, are those recommended in Ref. 8. Curve 3, corresponding to $\beta = 2.27 \text{ \AA}^{-1}$, is suggested as less likely but not ruled out in Ref. 8.) Also included are the calculated potential of Stevens *et al.* from Ref. 28 (long dashed curve), and that of Jeung *et al.* from Ref. 29 (short dashed curve). The solid curve for $R > 4.5 \text{ \AA}$ is the experimental bound portion of the $1^3\Sigma^+$ state from Ref. 16. In this figure, the energy zero is taken as the $\text{Na}(3s) + \text{K}(4s)$ dissociation limit.

the $2^3\Pi(v=13)$ level to be 3.53 \AA which compares with LeRoy's turning point of $\sim 3.38 \text{ \AA}$. We believe this $\sim 0.15 \text{ \AA}$ shift of LeRoy's $2^3\Pi$ inner turning point is consistent with the similar shift in their $1^3\Sigma^+$ potential. We note that the results of Kowalczyk,³⁰ Kato and Noda,⁴ and the present work all seem to be mutually consistent. The bound-free portion of Breford and Engelke's $2^3\Pi(v=13, J=14) \rightarrow 1^3\Sigma^+$ spectrum (using Kato and Noda's assignment) is extremely well reproduced using Kowalczyk's $2^3\Pi$ potential and the $1^3\Sigma^+$ potential of the present work (see Fig. 10). This is strong confirmation of the analysis presented here.

D. Relative transition dipole moment function $D(R)$

The transition dipole moment function $D(R)$ is reflected in the relative intensities of the various maxima in the oscillating continua. However, determination of this function proved to be more difficult than that of the $1^3\Sigma^+$ state potential. Initially, we tried to use the CFCA to directly relate a particular emission wavelength to a particular R . Since the CFCA assumes that the dipole moment varies slowly enough to be pulled out of the integral in Eq. (2), the intensity is proportional to $|D(R)|^2$. We could then obtain a relative dipole moment function, $D(R)^{\text{rel}}$, from the following formula⁸:

$$D(R)^{\text{rel}} = \left[\frac{I(\lambda)^{\text{obs}}}{I(\lambda)^{(D=1)}} \right]^{1/2}. \quad (6)$$

This procedure, when based upon the CFCA, proved unsuccessful. The problem occurs because the CFCA assumes that the wave function overlap is localized at a particular R , when in fact it occurs over a relatively broad region of R . This means that a fairly wide region of R contributes to each emission wavelength. In fact, the dipole moment at any R can contribute to several intensity maxima in a given spectrum. A trial and error approach is also unsatisfactory, as it is not

obvious how to adjust $D(R)$ to correct for errors in the calculated spectrum.

Our eventual resolution of these difficulties came from looking at accumulated overlap integrals similar to those shown in Fig. 4. These tell us the range of R values which contribute to a given wavelength. We model this range as a square "window" which was determined for each peak in the spectra. The average R of each of these windows then relates the internuclear separation to a corresponding λ , similar to the CFCA. However, these $R(\lambda)$'s are not the same as those given by the CFCA. As in the CFCA, we have assumed that $D(R)$ is sufficiently slowly varying to allow it to be removed from within the integral of Eq. (2). Since these integration windows are broad, they will wash out any small details in $D(R)$. Thus we were unable to determine such details using a formula equivalent to Eq. (6). Instead we modeled the dipole moment by a linear function $D(R) = m(R - R_0) + D_0$ and determined a best value for the parameter m . Since only relative dipole moments were determined in the experiment, these results were normalized to the theoretical value²⁷ $D(R_0) = D_0 = 1.07 \text{ a.u.}$ for $R_0 = 8.034 \text{ a.u.}$ The fitting procedure was as follows. Each set of relative dipole moments, corresponding to a particular spectrum, was fit by a linear function which was then normalized to the value $D(R_0) = D_0$. Once all the dipole moment sets were placed on the same scale, the entire set of points was fit to the function $D(R) = m(R - R_0) + D_0$. The determined best value for m is 0.121 ± 0.029 in atomic units, valid for the range $7.5 < R < 8.9 \text{ a.u.}$ ($4 < R < 4.7 \text{ \AA}$). This transition dipole moment is plotted in Fig. 11, where it is compared to the theoretical result of Ratcliff *et al.*²⁷ We should note that the error bars on the parameter m above are purely statistical, but that the biggest error in our procedure is clearly the assumed linear form of $D(R)$. Nevertheless, the technique, which was adapted from LeRoy *et al.*,⁸ is capable of providing a reasonable experimental picture of the

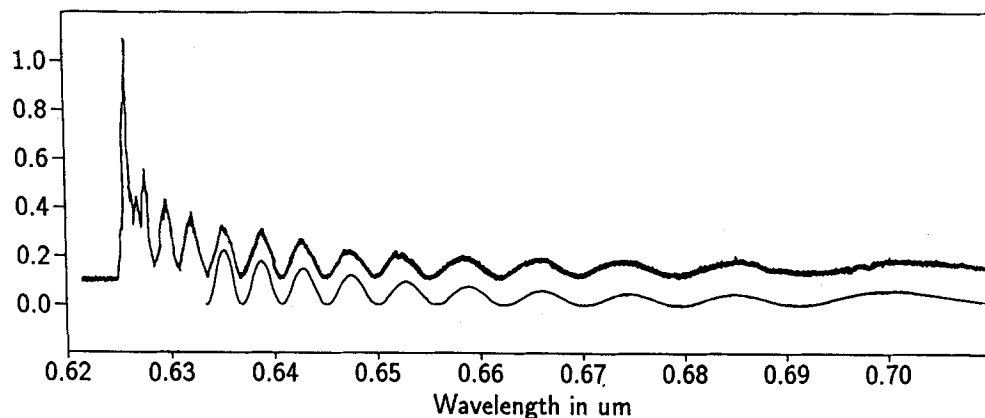


FIG. 10. Comparison of Breford and Engelke's (Ref. 1) $2^3\Pi(v=13, J=14) \rightarrow 1^3\Sigma^+$ bound-free emission [assignment from Kato and Noda (Ref. 4)] with spectrum calculated using Kowalczyk's (Ref. 30) $2^3\Pi$ potential and the $1^3\Sigma^+$ potential from the present work. The transition dipole moment was taken from Ratcliff *et al.* (Ref. 27). Only the ten maxima shown in the calculated spectrum represent bound-free emission (Refs. 4 and 8). The remaining maxima in the experimental trace correspond to bound-bound emission into the $1^3\Sigma^+$ state van der Waals well.

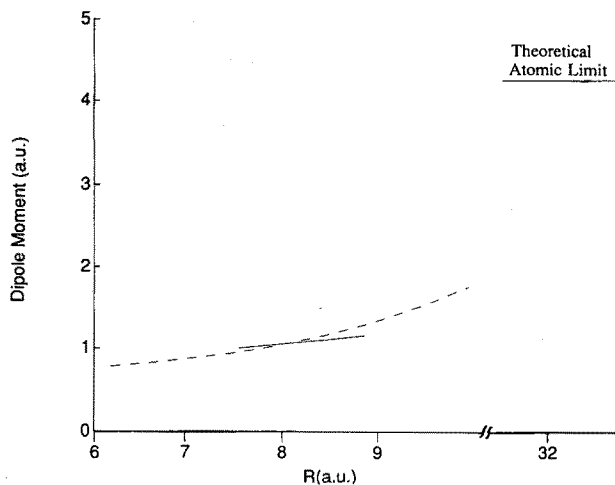


FIG. 11. Comparison of the relative dipole moment obtained in the present work (solid line) with the theoretical dipole of Ratcliff *et al.* (Ref. 27) (dashed line). The experimental $D(R)$ was normalized to the Ratcliff *et al.* result at $R = 8.034$ a.u. The flat line of the theoretical curve to the right represents the asymptotic theoretical dipole moment.

relative dipole moment function. It would be of greater value in cases where the available data cover a larger range of R values.

Figure 12 shows a comparison of several experimental spectra with the relevant simulated spectra calculated using the $1^3\Sigma^+$ repulsive wall determined as outlined in the previous section and the transition dipole moment determined as discussed in this section.

E. Comparison of "exact" experimental $1^3\Sigma^+$ potential to results of reflection approximations

There has been much interest in reflection approximations and efforts have been made to find a new reflection method which will correctly give the positions of the maxima and minima of bound-free spectra. In their very recent paper, Eryomin and Kuz'menko³¹ have developed several new methods for determining bound-free spectra by reflection of the upper bound state nuclear probability function $[\chi_U^*(R)\chi_U(R)]$. Of the three methods proposed, one permits the straightforward inversion of bound-free spectra to determine the lower unbound state potential, if the upper state potential and energy level are known. The method lies between the two semiclassical approximations previously described; the CFCA and the delta-function approximation.

Rather than conserving all the initial state kinetic energy as in the CFCA, or losing all kinetic energy as in the delta-function approximation, the Eryomin and Kuz'menko method retains one third of the kinetic energy:

$$\frac{hc}{\lambda} = E_U - \{V_L(R) + \frac{1}{3}[E_U - V_U(R)]\}, \quad (7)$$

with E_U = the upper state energy, V_U = the upper state potential, and V_L = the lower state potential. As in the other two approximations, the emission intensity is proportional to the probability that the atomic pair is separated by the appropriate R . This approximation is justified by the reason-

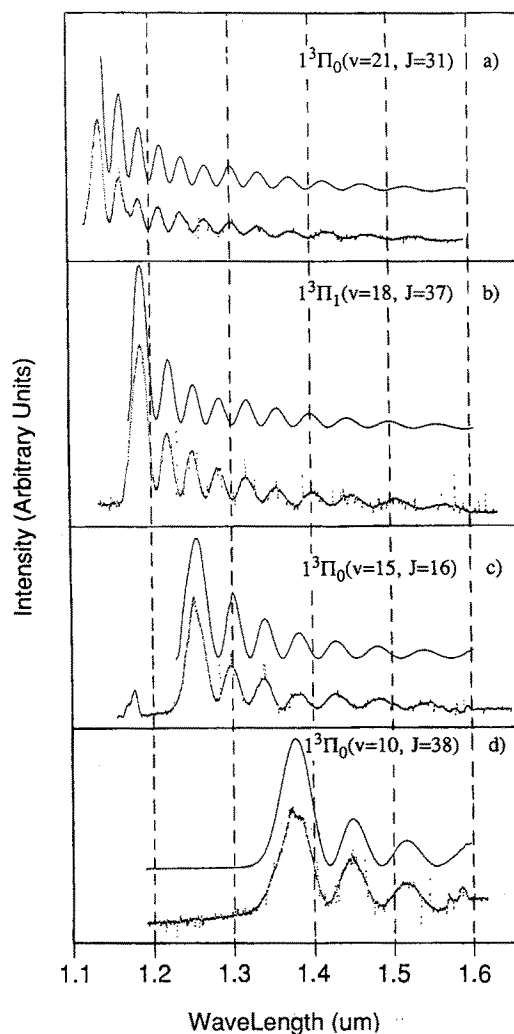


FIG. 12. Comparison of quantum-mechanical calculated spectra with experimental spectra. Each spectrum was generated from a single rovibrational level of the $1^3\Pi_\Omega$ states: (a) $\Omega = 0, v' = 21, J' = 31$. (b) $\Omega = 1, v' = 18, J' = 37$. (c) $\Omega = 0, v' = 15, J' = 16$. (d) $\Omega = 0, v' = 10, J' = 38$. In part (a) the first peak in the calculated spectrum is cut off, since that part of the spectrum represents bound-bound $1^3\Pi_0 \rightarrow 1^3\Sigma^+$ emission which is not handled by the program BOUND-FREE. The small feature at $1.17 \mu\text{m}$ in trace (c) is a potassium atomic line.

ing that the first large maximum of the lower state wave function (which contributes most to the radial overlap integral) does not occur at the turning point (as assumed in the delta-function approximation), but is located between the turning point and the momentum conservation point. The effect of this offset is approximated by the preservation of one third of the kinetic energy. It can be seen that this approximation is intermediate between the CFCA and the delta-function approximations. Figure 13 compares the potentials determined using the CFCA, the delta-function approximation, and the Eryomin and Kuz'menko approximation with the potential determined here by fully quantum mechanical methods. Figure 3 shows a comparison of spectra calculated using the delta function approximation, the CFCA, the Eryomin and Kuz'menko approximation, and a fully quantum mechanical calculation, for fixed potential curves.

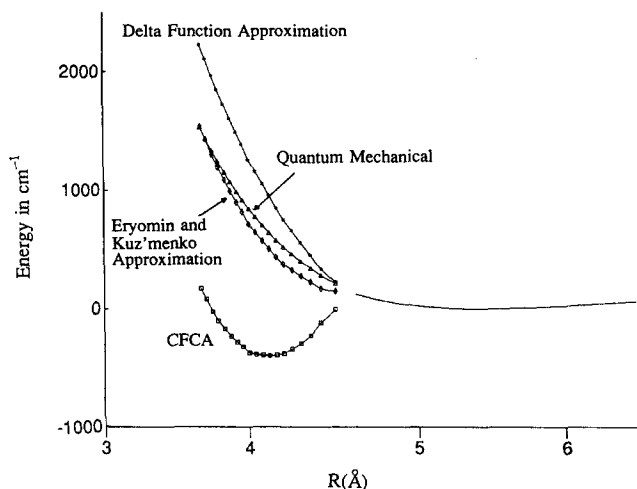


FIG. 13. $1^3\Sigma^+$ state potentials calculated from the various reflection techniques using the observed $1^3\Pi_1(v=18, J=37) \rightarrow 1^3\Sigma^+$ spectrum, and compared to the quantum-mechanical result of the present work. In each case, the rotational energy was subtracted off to yield rotationless potentials.

We should comment specifically on the very poor performance of the CFCA in Fig. 13 where it does not even correctly predict the repulsive nature of the $1^3\Sigma^+$ state. In any of the reflection methods, the function $\lambda(R)$ is uniquely determined by the experimental spectrum and the bound upper state wave function (i.e., maxima and minima of the spectrum correspond uniquely to antinodes and nodes of the wave function). Thus the repulsive state potential is directly determined by the function $\lambda(R)$ and the fraction of the kinetic energy which is preserved by the particular reflection method (0 for the delta function, 33.3% for the Eryomin and Kuz'menko approximation, and 100% for the CFCA). The actual potential will generally be bounded by the two extreme cases (the delta function and CFCA) which in turn must differ by exactly the upper state kinetic energy at each R . Child *et al.*⁷ point out that reflection methods work best when the de Broglie wavelength of the bound state wave function is much longer than the free state wave function in the region near its turning point. This occurs for low v bound state energies, a steep repulsive curve, and high free state energies. Under such conditions, the derived delta-function approximation and CFCA potentials will lie close together. In Fig. 13, we inverted a spectrum originating from $v' = 18$ in which the kinetic energy is greater than 2000 cm^{-1} . These spectra are also sensitive to a region of the lower state potential where the slope is not very steep. Thus this is a severe test of the reflection methods.

The quantum mechanical results can perhaps best be compared to the reflection methods by calculating the fraction of the kinetic energy preserved at each R from the function $\lambda(R)$ and the quantum mechanical lower state potential (i.e., we treat the quantum result as if it were a reflection method and determine the fraction of kinetic energy preserved). For the case of $1^3\Pi_1(v=18, J=37) \rightarrow 1^3\Sigma^+$ emission (Fig. 13) this fraction ranges from 5% to 34%. In comparison, for $v' = 21, J' = 31$ and $v' = 10, J' = 38$ the corresponding fractions range from 5% to 30% and 15% to

30%. We have made similar calculations for Kato and Noda's $2^3\Pi(v=13, J=14) \rightarrow 1^3\Sigma^+$ emission,⁴ the synthetic $\text{Br}_2 \text{X } 1^1\Sigma_g^+(v=5, J=0) \rightarrow 1^1\Pi_{1u}$ spectrum of LeRoy *et al.*⁸ and the synthetic Kr_2 spectra of Eryomin and Kuz'menko.³¹ In these cases, the fraction of kinetic energy preserved typically ranges from 10 to 50%. Thus it can be seen that the one-third kinetic energy prescription of Eryomin and Kuz'menko is indeed an improvement over the delta function approximation and the CFCA, but is still only an approximation. The actual level of agreement depends strongly on the details of the potentials.

V. CONCLUSION

In summary, we have observed NaK $1^3\Pi_\Omega \rightarrow 1^3\Sigma^+$ bound-free emission from specific rovibrational levels of the $1^3\Pi_\Omega$ states. We have carried out quantum mechanical simulations of the emission spectra based upon previously determined experimental potentials for the $1^1\Sigma^+, 2^1\Sigma^+, 1^3\Pi_1$, and $1^3\Sigma^+$ states, and the $1^3\Pi$ fine-structure constant. Using these simulations, we were able to fit the repulsive wall of the $1^3\Sigma^+$ state above the dissociation limit by a potential of the form $Ae^{-BR} + C$. In addition, this potential, combined with the $2^3\Pi$ state potential of Kowalczyk,³⁰ was able to accurately fit the NaK $2^3\Pi \rightarrow 1^3\Sigma^+$ bound-free spectrum of Breford and Engelke.¹ Finally, we were able to crudely determine the $1^3\Pi \rightarrow 1^3\Sigma^+$ relative transition dipole moment function by comparing measured relative intensities of the oscillatory bound-free emission maxima to those of simulations. In the latter, a linear dependence $D(R) = m(R - R_0) + D_0$ was assumed.

At present, we are involved in extending our detection system's sensitivity further to the red in order to extend our experimental $1^3\Sigma^+$ potential to shorter R . We also hope to determine the lifetimes of perturbed states, which will allow us to place our experimental dipole moment function on an absolute basis. Finally, we are in the process of determining the perturbation strength, ξ_{el} by finding both levels of each mutually perturbing pair.

ACKNOWLEDGMENTS

We would like to thank Dr. Joel Tellinghuisen and Dr. Robert LeRoy for useful discussions and Dr. Amanda Ross for providing us with unpublished results. We would also like to thank Mr. Michael Miller for technical assistance. This work was supported by the U. S. Army Research Office under Grants DAAL03-86-K-0161 and DAAL03-89-K-0171, and the National Science Foundation under Grants PHY-8451279 and CHE 86-17954. In addition, we are grateful for equipment provided under the Defense University Research Instrumentation Program, Grant DAAL03-88-0063.

¹E. J. Breford and F. Engelke, *Chem. Phys. Lett.* **53**, 282 (1978).

²E. J. Breford and F. Engelke, *J. Chem. Phys.* **71**, 1994 (1979).

³D. Eisel, D. Zevgolits, and W. Demtröder, *J. Chem. Phys.* **71**, 2005 (1979).

⁴H. Kato and C. Noda, *J. Chem. Phys.* **73**, 4940 (1980).

⁵J. Huennekens, T. G. Walker, and S. C. McClain, *J. Chem. Phys.* **83**, 4949 (1985).

- ⁶J. Huennekens, A. Loza, M. Masters, and K. M. Sando, *J. Chem. Phys.* **88**, 6013 (1988).
- ⁷M. S. Child, H. Essen, and R. J. LeRoy, *J. Chem. Phys.* **78**, 6732 (1983).
- ⁸R. J. LeRoy, W. J. Keogh, and M. S. Child, *J. Chem. Phys.* **89**, 4564 (1988).
- ⁹D. D. Konowalow and P. S. Julienne, *J. Chem. Phys.* **72**, 5815 (1980).
- ¹⁰O. C. Mullins, C. R. Mahon, and T. F. Gallagher, *Chem. Phys. Lett.* **126**, 501 (1986).
- ¹¹A. J. Ross, P. Crozet, C. Effantin, J. d'Incan, and R. F. Barrow, *J. Phys. B At. Mol. Phys.* **20**, 6225 (1987).
- ¹²L. Li and R. W. Field, *J. Mol. Spectrosc.* **123**, 237 (1987).
- ¹³H. Kato, M. Otani, and M. Baba, *J. Chem. Phys.* **89**, 653 (1988).
- ¹⁴C. Effantin, O. Babaky, K. Hussein, J. d'Incan, and R. F. Barrow, *J. Phys. B At. Mol. Phys.* **18**, 4077 (1985).
- ¹⁵A. J. Ross, C. Effantin, J. d'Incan, and R. F. Barrow, *J. Phys. B At. Mol. Phys.* **19**, 1449 (1986).
- ¹⁶A. J. Ross, C. Effantin, J. d'Incan, and R. F. Barrow, *Mol. Phys.* **56**, 903 (1985).
- ¹⁷A. J. Ross, R. M. Clements, and R. F. Barrow, *J. Mol. Spectrosc.* **127**, 546 (1988).
- ¹⁸P. S. Herman and K. M. Sando, *Program Bound-Free*, University of Iowa, Department of Chemistry (unpublished).
- ¹⁹P. S. Herman and K. M. Sando, *J. Chem. Phys.* **68**, 1153 (1978).
- ²⁰E. U. Condon, *Proc. Natl. Acad. Sci.* **13**, 462 (1927).
- ²¹R. S. Mulliken, *J. Chem. Phys.* **55**, 309 (1971).
- ²²J. Tellinghuisen, *J. Mol. Spectrosc.* **103**, 455 (1984).
- ²³C. R. Vidal and J. Cooper, *J. Appl. Phys.* **40**, 3370 (1969).
- ²⁴R. Stair, W. E. Schneider, and J. K. Jackson, *Appl. Opt.* **2**, 1151 (1963).
- ²⁵A. J. Ross (private communication).
- ²⁶G. Herzberg, *Molecular Spectra and Molecular Structure: I. Spectra of Diatomic Molecules* (Van Nostrand Reinhold Company, New York, 1950).
- ²⁷L. B. Ratcliff, D. D. Konowalow, and W. J. Stevens, *J. Mol. Spectrosc.* **110**, 242 (1985).
- ²⁸W. J. Stevens, D. D. Konowalow, and L. B. Ratcliff, *J. Chem. Phys.* **80**, 1215 (1984).
- ²⁹G.-H. Jeung, J.-P. Daudey, and J.-P. Malrieu, *Chem. Phys. Lett.* **94**, 300 (1983).
- ³⁰P. Kowalczyk, *J. Mol. Spectrosc.* **136**, 1 (1989).
- ³¹V. V. Eryomin and N. E. Kuz'menko, *Chem. Phys.* **136**, 127 (1989).